

# Effect of Hydraulic Resistivity on a Weakly Nonlinear Thermal Flow in a Porous Layer

D. Bhatta<sup>1†</sup> and D. N. Riahi<sup>2</sup>

<sup>1</sup>The University of Texas Rio Grande Valley, Edinburg, TX, USA, 78539

<sup>2</sup>The University of Texas Rio Grande Valley, Brownsville, TX, USA, 78520

†Corresponding Author Email: [dambaru.bhatta@utrgv.edu](mailto:dambaru.bhatta@utrgv.edu)

(Received February 27, 2019; accepted July 24, 2019)

## ABSTRACT

Heat and mass transfer through porous media has been a topic of research interest because of its importance in various applications. The flow system in porous media is modelled by a set of partial differential equations. The momentum equation which is derived from Darcy's law contains a resistivity parameter. We investigate the effect of hydraulic resistivity on a weakly nonlinear thermal flow in a horizontal porous layer. The present study is a realistic study of nonlinear convection flow with variable resistivity whose rate of variation is arbitrary in general. This is a first step for considering more general problems in applications that involve variable resistivity that may include both variations in permeability and viscosity of the porous layer. Such problems are important for understanding properties of underground flow, migration of moisture in fibrous insulations, underground disposal of nuclear waste, welding process, petrochemical generation, drug delivery in vascular tumor, etc. Using weakly non-linear procedure, the linear and first-order systems are derived. The critical Rayleigh number and the critical wave number are obtained from the linear system using the normal mode approach for the two-dimensional case. The linear and first-order systems are solved numerically using the fourth-order Runge-Kutta and shooting methods. Numerical results for the temperature are presented in tabular and graphical forms for different resistivities. Through this study, it is observed that a stabilizing effect on the dependent variables occurs in the case of a positive vertical rate of change in resistivity, whereas a destabilizing effect is noticed in the case of a negative vertical rate of change in resistivity. The results obtained indicate that the convective flow due to the buoyancy force is more effective for weaker resistivity.

**Keywords:** Hydraulic resistivity; Weakly nonlinear; Hydro-thermal; Convective flow; Rayleigh number.

## NOMENCLATURE

$P$	perturbed pressure	$(x,y,z)$	cartesian coordinates
$p$	pressure	$\vec{u}$	perturbed velocity vector
$p_b$	basic state pressure	$U$	X component of the velocity vector
$\varepsilon$	perturbation parameter	$V$	y component of the velocity vector
$i$	complex unit	$W$	z component of the velocity vector
$k$	unit vector in the vertical positive z-direction	$\vec{u}$	velocity vector
$\mathcal{R}$	Rayleigh number	$\vec{u}_b$	basic state velocity vector
$\mathcal{R}_c$	critical Rayleigh number	$\alpha$	wavenumber
$T$	temperature	$\gamma$	resistivity
$\Theta$	perturbed temperature	$\gamma_0$	rate of change in resistivity
$\theta_b$	basic state temperature	$\nabla^2$	3D Laplacian
$t$	time variable	$\Delta_2$	2D Laplacian

## 1. INTRODUCTION

Fluid flow and heat transfer through a porous medium have been a topic of research interest for last

several decades. A porous medium is a material that consists of a solid material with inter-connected voids or pores. It is characterized by its porosity and the permeability of the medium is the. Darcy's law

for porous media is taken into account in the momentum equation, which is similar to the Navier-Stokes equation. In natural porous media the distribution of pores with respect to shape and size is not regular. But in typical experiments the quantities of interest are measured over areas that cross many pores and changes of such space averaged quantities may be considered in a regular way and hence are acceptable to theoretical

treatment. Heat transfer through a porous medium is a very common phenomenon. The normal tendency of a fluid to expand due to heating causes a density inversion to occur, if the heating is strong enough, a circulatory motion follows, termed convection. Convection in fluid media is well-studied phenomenon and occurs in many natural settings and in many industrial applications. Mathematical treatment and research on convection in porous media have been presented by many authors through many research articles (Nield and Bejan 2017, Vafai 2005).

Many studies have been presented by various authors to investigate convection in porous media with varying porosity or permeability. Rubin (1981) investigated the onset of thermohaline convection in a porous medium with varying hydraulic resistivity. Vafai (1984) investigated wall effects due to variable porosity. Variable porosity and thermal dispersion effects due to natural convection in an inclined porous cavity were studied by Hsiao (1998). Modal package convection for a porous medium with boundary imperfections was analyzed by Riahi (1996). The effect of variable permeability in porous media was analyzed analytically and numerically by Rees and Pop (2000). Hassanien and Omer (2005) studied the effect of variable permeability in a porous medium. Oliveski and Macrczak (2008) analyzed the effect of variable porosity and Darcy number in a porous cavity. A medium with variable permeability was analyzed by Aldoss (2009). Linear and nonlinear stability for a rotating porous fluid layer was analyzed by Falsaperla *et al.* (2010). Investigations of Darcy's law for the flow with Pressure-dependent viscosity in a porous medium were carried out several researched including Nakshatrala and Rajagopal (2011), Fusi, Farina and Rosso (2015). The onset of Bernard-Marangoni convection in composite layers with anisotropic porous material was studied by Gangadharaiah (2016).

Riahi (1989) carried out nonlinear stability analysis in a porous layer with permeable boundaries. The case of a continuous finite bandwidth of convection modes in a horizontal layer was analyzed by Riahi (1996). Convective flows, in a horizontal dendritic porous layer (also known as mushy layer) during alloy solidification, are known to produce undesirable effects in the final form of the alloy. Study on oscillatory modes of nonlinear compositional convection in mushy layers was carried out by Riahi (2009). Muddamallappa *et al.* (2009) used a modified mushy layer model based on the standard near eutectic approximation. They used linear stability analysis and calculated critical

Rayleigh number for the cases of both constant and variable permeability. However, the issues of nonlinear effects and transition effects on the chimney formation did not feature in their investigation. Bhatta *et al.* (2010) studied weakly nonlinear convective flow in an active (variable permeability) mushy layer with permeable mush-liquid interface. Bhatta *et al.* (2012) studied weakly nonlinear convective flows in mushy layers with and without the magnetic effect and permeable mush-liquid interface.

A model for an aquifer which can be treated as porous media was presented by Fowler (1997). Rubin (1982) used Galerkin method to analyze the effects of hydraulic resistivity and thermal diffusivity on stability in a nonhomogeneous aquifer. Bhatta and Riahi (2017) investigated weakly nonlinear hydro-thermal two-dimensional convective flow in a horizontal aquifer by treating it as porous medium. Their investigation was limited to small linear vertical variations in the permeability and thermal conductivity. Wang *et al.* (2017) presented proper orthogonal decomposition (POD) reduced-order model to solve heat transfer problem for heat exchanger. Recently, Dejam (2018, 2019a, 2019b, 2019c), and Kou and Dejam (2019) presented a series of research work in porous media.

There have been some research studies on the effect of hydraulic resistivity (Rubin 1981; Bhatta and Riahi 2017) as well as related ones on variable permeability with or without magnetic field (Bhatta *et al.* 2010, 2012). Bhatta *et al.* (2010, 2012) studied nonlinear convective flow in a mushy layer, which is a porous layer formed between the solid and liquid layers during the solidification process of binary alloy. The mushy layer that they considered has variable permeability and hence variable resistivity, and they determine the flow evolution for both cases in the absence or presence of a vertically oriented magnetic field. Bhatta and Riahi (2017) studied convective flow in an aquifer layer with variable resistivity, by under the condition that the rate of change of the resistivity was sufficiently small. Tait *et al.* (1992) carried out experimental investigation of convective flow in a mushy layer and determined the preferred planform of three-dimensional compositional convection in a mushy layer with variable permeability.

Under severe restriction of small variation, previous theoretical studies determined convective flow velocity and temperature for different parameter values. In this paper, we use weakly nonlinear procedure to investigate the effect of the vertical rate of change of resistivity on the solutions for a hydro-thermal convective flow in a horizontal porous medium. The present study is to understand the effects of resistivity variations on the non-linear convective flow, which is a first step for more general problems involving resistivity variations. Such problems are important for understanding properties of underground flow, migration of moisture in fibrous insulations, underground disposal of nuclear waste, welding process, petrochemical generation, drug delivery in vascular

tumor etc. We determine important results, in particular, we found that the convective flow is effective if the resistivity is weak and vice versa a strong resistivity leads to weak flow.

We present the mathematical formulation in section 2 where all the important mathematical equations are derived. Section 3 elaborates the solution procedure with the usage of weakly nonlinear method. Normal mode approach for the two dimensional case is derived in section 4. Numerical results and discussion are presented in section 5. Section 6 summarizes the procedure and conclusions of this study. Some derivations of the main equations presented in section 3 are added in the Appendix.

## 2. MATHEMATICAL FORMULATION

Here, we consider a horizontal porous medium bounded above and below by impermeable boundaries and heated from below. The horizontal  $xy$ -plane is taken as the bottom boundary of the medium, and  $z$ -axis is vertical and positive upward. The geometry of the physical system is shown in Fig.1.

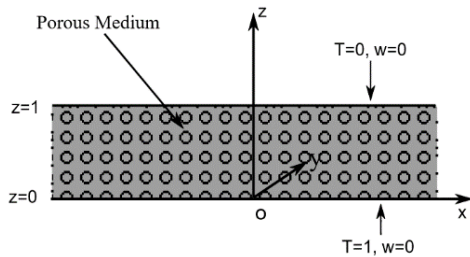


Fig. 1. A sketch of physical system.

The governing equation for nondimensional system can be expressed as (Rubin 1982)

$$\nabla \cdot \vec{u} = 0 \quad (1)$$

$$\gamma \vec{u} - \mathcal{R}T\hat{k} + \nabla p = 0 \quad (2)$$

$$\frac{\partial T}{\partial t} + \vec{u} \cdot \nabla T = \nabla^2 T \quad (3)$$

Here  $\vec{u}$ ,  $\gamma$ ,  $T$ ,  $p$ ,  $\mathcal{R}$ ,  $t$  and  $\hat{k}$ , respectively, represent the velocity, resistivity, temperature, pressure, Rayleigh number, time and unit vector in the upward vertical direction. This system consists of the continuity equation, the Darcy equation and the heat equation. For steady state solution, all dependent variables ( $\vec{u}$ ,  $T$ ,  $p$ ) are functions of  $x, y, z$ . Here, we assume a linear vertical variation in resistivity  $\gamma$  as

$$\gamma = 1 + \gamma_0 z, \quad (4)$$

where  $\gamma_0$  is a constant which is the vertical rate of change of the resistivity. The boundary conditions are

$$T = 1, w = 0 \quad \text{at } z = 0 \quad (5)$$

$$T = 0, w = 0 \quad \text{at } z = 1 \quad (6)$$

where  $w$  is the vertical  $z$ -component of  $\vec{u}$ . A schematic diagram of the convection caused by the

heat difference between the bottom and top layers is shown in Fig.2.

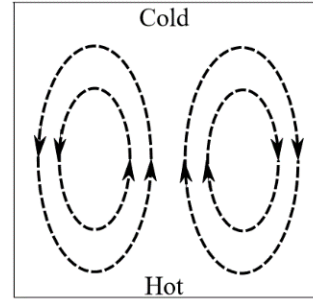


Fig. 2. Convection due to a heated bottom.

## 3. SOLUTION PROCEDURE

We perturb the system given by (1-3) as follows

$$[T, \vec{u}, p] = [\theta_b(z), \vec{u}_b(z), p_b(z)] + \varepsilon [\theta(x, y, z), \vec{u}(x, y, z), P(x, y, z)]. \quad (7)$$

Here,  $\theta_b, \vec{u}_b, p_b$  are the basic steady state solutions of system with no flow and  $\theta, \vec{u}, P$  are perturbed solutions. The perturbation parameter is given by  $\varepsilon = (\mathcal{R} - \mathcal{R}_c) / \mathcal{R}_1 > 0$  i.e.,  $\mathcal{R} = \mathcal{R}_c + \varepsilon \mathcal{R}_1$ , where  $\mathcal{R}_c$  is the critical Rayleigh number and  $\mathcal{R}_1$  is the nonlinear contribution to  $\mathcal{R}$  beyond the critical number.

### 3.1 Basic State System and its Solutions

Using (7) in (1) through (3) and by comparing the coefficients of  $\varepsilon^0$  as the basic state system with no flow, we have

$$\frac{d^2 \theta_b}{dz^2} = 0, \quad \frac{dp_b}{dz} - \mathcal{R}_c \theta_b = 0, \quad \vec{u}_b = \vec{0} \quad (8)$$

with boundary conditions  $\theta_b = 1$  at  $z = 0$  and  $\theta_b = 0 = p_b$  at  $z = 1$ . Now, by solving the basic state system (8), we can express the solutions as

$$\theta_b = 1 - z, \quad p_b = -\frac{\mathcal{R}_c}{2} (1 - z)^2, \quad \vec{u}_b = \vec{0}.$$

### 3.2 Perturbed System

Using (7) in the system given by (1-3), we obtain a system in terms of the perturbed variables as follows:

$$\nabla \cdot \vec{u} = 0 \quad (9)$$

$$\gamma \vec{u} - \mathcal{R}_c \theta_b \hat{k} + \nabla P = \varepsilon \mathcal{R}_1 \theta \hat{k} \quad (10)$$

$$\nabla^2 \theta - \vec{u} \cdot \nabla \theta_b = \varepsilon \vec{u} \cdot \nabla \theta \quad (11)$$

and the boundary conditions become  $\theta = W = 0$  at  $z = 0, 1$ . Here,  $W$  is the vertical  $z$ -component of  $\vec{u}$ .

Now, expressing  $\theta(x, y, z)$  and  $W(x, y, z)$  as

$$\theta = \theta_0 + \varepsilon \theta_1 + \varepsilon^2 \theta_2 + \dots \quad (12)$$

$$W = W_0 + \varepsilon W_1 + \varepsilon^2 W_2 + \dots \quad (13)$$

and the work shown in the Appendix, we obtain different order systems, namely, the linear and the

first-order. Subindex is used to denote various orders.

### 3.2.1 Linear System

Putting  $\Theta$ ,  $W$  given by (12), (13) in the Eqs. (25) and (26) given in the Appendix, the linear system can be expressed by the following equations:

$$\gamma \nabla^2 W_0 + \frac{d\gamma}{dz} (DW_0) - \mathcal{R}_c (\Delta_2 \theta_0) = 0 \quad (14)$$

$$\nabla^2 \theta_0 - W_0 \frac{d\theta_0}{dz} = 0, \quad (15)$$

with the boundary conditions  $\theta_0 = W_0 = 0$  at  $z = 0, 1$ .

### 3.2.2 First-Order System

Putting  $\Theta$ ,  $W$  given by (12), (13) in the Eqs. (25) and (26), the first-order system can be expressed as:

$$\gamma \nabla^2 W_1 + \frac{d\gamma}{dz} (DW_1) - \mathcal{R}_c (\Delta_2 \theta_1) = \mathcal{R}_1 (\Delta_2 \theta_0) \quad (16)$$

$$\nabla^2 \theta_1 - W_1 \frac{d\theta_1}{dz} = \vec{U}_0 \cdot \nabla \theta_0 \quad (17)$$

and the boundary conditions are  $\theta_1 = W_1 = 0$  at  $z = 0, 1$ .

## 4. 2-D SOLUTIONS: NORMAL MODE APPROACH

Now, we consider the two dimensional case. Using the normal mode approach, we take the following forms for the linear solutions

$$\theta_0(x, z), W_0(x, z) = [\theta_0(z), W_0(z)] e^{i\alpha x}, \quad (18)$$

where  $\alpha$  denotes the wave number. As derived in the Appendix, the normal mode linear solutions satisfy

$$(1 + \gamma_0 z) \left( \frac{d^2}{dz^2} - \alpha^2 \right) \widehat{W}_0 + \gamma_0 \frac{d\widehat{W}_0}{dz} + \alpha^2 \mathcal{R}_c \widehat{\theta}_0 = 0 \quad (19)$$

$$\left( \frac{d^2}{dz^2} - \alpha^2 \right) \widehat{\theta}_0 - \widehat{W}_0 \frac{d\widehat{\theta}_0}{dz} = 0 \quad (20)$$

with boundary conditions  $\widehat{\theta}_0 = \widehat{W}_0 = 0$  at  $z = 0, 1$ .

For the normal mode first-order solutions, we have two parts: one is called one-alpha mode due to the presence of  $e^{i\alpha x}$  and the other called two-alpha mode due to the presence of  $e^{2i\alpha x}$ . These satisfy (as derived in the Appendix)

$$(1 + \gamma_0 z) \left( \frac{d^2}{dz^2} - \alpha^2 \right) \widehat{W}_{11} + \gamma_0 \frac{d\widehat{W}_{11}}{dz} + \alpha^2 \mathcal{R}_c \widehat{\theta}_{11} = -\alpha^2 \mathcal{R}_c \widehat{\theta}_0 \quad (21)$$

$$\left( \frac{d^2}{dz^2} - \alpha^2 \right) \widehat{\theta}_{11} + \widehat{W}_{11} = 0 \quad (22)$$

with  $\widehat{\theta}_{11} = \widehat{W}_{11} = 0 = 0$  at  $z = 0, 1$  and

$$(1 + \gamma_0 z) \left( \frac{d^2}{dz^2} - 4\alpha^2 \right) \widehat{W}_{12} + \gamma_0 \frac{d\widehat{W}_{12}}{dz} + 4\alpha^2 \mathcal{R}_c \widehat{\theta}_{12} = 0 \quad (23)$$

$$\left( \frac{d^2}{dz^2} - \alpha^2 \right) \widehat{\theta}_{12} + \widehat{W}_{12} = \widehat{W}_0 \frac{d\widehat{\theta}_0}{dz} \quad (24)$$

with  $\widehat{\theta}_{12} = \widehat{W}_{12} = 0 = 0$  at  $z = 0, 1$ .

## 5. NUMERICAL RESULTS AND DISCUSSION

In obtaining the numerical solutions, the fourth-order Runge-Kutta method (RK4) is used in combination with the shooting method (Kincaid and Cheney, 2002). Runge-Kutta methods are numerical procedures used to solve a first-order ordinary differential equation (ODE) with a given initial value, i.e., to solve an IVP (initial value problem). These methods are also used to solve a system of first-order ordinary differential equations with given initial conditions. Higher-order ODE can be solved by expressing the ODE as a system of first-order ODEs. Advantages of Runge-Kutta methods over Taylor's series methods are that they do not require computation and evaluation of the derivatives which can be very complicated and time consuming. In this work, we use the fourth-order Runge-Kutta method (RK4). It is widely used due to its simplicity in implementation and higher-order accuracy up to the fourth-order. Higher-order Runge-Kutta methods are less attractive than the classical fourth-order due to a higher number of function evaluations. The shooting method is a numerical method used to solve a boundary value problem (BVP) by converting it to an IVP. This method allows one to shoot out trajectories for possible solutions in different directions until a trajectory that has the given boundary values is found. For solving the ODE systems appearing in this work, the codes are written in the Java programming language and for graphing the results, MATLAB is used.

To obtain the critical Rayleigh number and wave numbers, we solve the linear system (19)-(20). We use the fourth order Runge-Kutta method together with the shooting method for a particular value of  $\gamma_0$  by varying the wave number and Rayleigh number and then obtain the minimum Rayleigh number (which is called the critical Rayleigh number), and the corresponding wave number (known as the critical wave number). The critical Rayleigh numbers and the critical wave numbers obtained numerically for different values of  $\gamma_0$  are shown in Table-1.

It is observed from the Table-1 that higher resistivity is stabilizing while smaller resistivity is destabilizing. When the rate of change in resistivity,  $\gamma_0$ , is zero, it reduces to the standard problem of constant resistivity where the critical wave number and critical Rayleigh number are known to be  $\pi$  and  $4\pi^2$ , respectively, which match the values computed in Table-1 (3rd column).

**Table 1 Critical wave numbers and Rayleigh numbers**

$\gamma_0$	-0.5	0.0	0.6	1.4
$\alpha_c$	3.14021	3.14159	3.14095	3.13928
$\mathcal{R}_c$	28.95956	39.47842	50.79039	64.83265

The marginal stability curves for different values of  $\gamma_0$  are displayed in Fig.3.

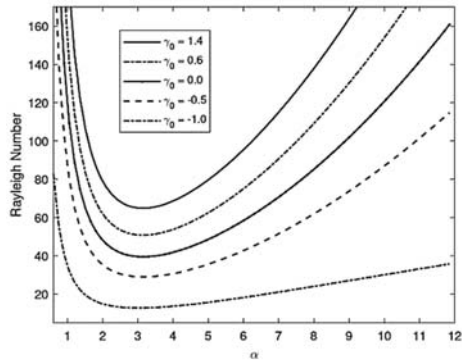


Fig. 3. Marginal stability curves for various  $\gamma_0$ .

The marginal stability curves make it clear that stability region is effected by  $\gamma_0$ , the vertical rate of change in resistivity. For smaller resistivity parameter, unstable region increases. Higher resistivity parameter implies higher stability.

Table-2 displays the linear solutions  $\widehat{\theta}_0(z)$  for  $\gamma_0 = 0.0, 0.6$  and  $-0.5$ . It is observed from our computational work that the linear solution,  $\widehat{\theta}_0(z)$ , has the maximum value of 0.01613 at  $z = 0.5$  for  $\gamma_0=0$ , and it is symmetric about the middle of the layer,  $z = 0.5$ . It has a maximum value of 0.02040 at  $z =0.53$  for  $\gamma_0 = -0.5$ , and a maximum value of 0.01337 at  $z=0.48$  for  $\gamma_0 = 0.6$ .

The linear solutions for the temperature,  $\widehat{\theta}_0(z)$ , for different values of  $\gamma_0$  are presented in Fig.4.

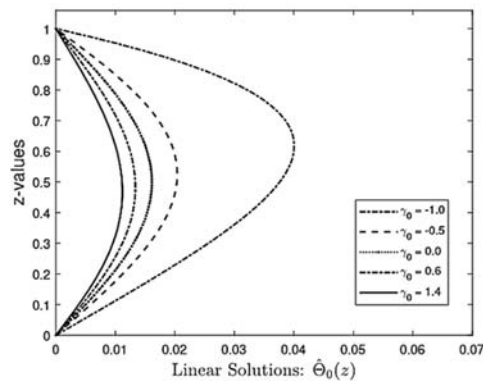


Fig. 4. Linear  $\widehat{\theta}_0(z)$  for various  $\gamma_0$ .

From Fig.4, it is observed that for  $\gamma_0 = 0.0$ , the temperature has a maximum value at the middle of the layer, i.e., at  $z = 0.5$  and temperature is symmetric about the middle of the layer. The maximum value of the temperature shifts downward in the layer for positive values of  $\gamma_0$  and the maximum value of the temperature moves upward for negative values of  $\gamma_0$ .

As fluid is moving upward due to the convection process, the flow amplitude reaches a maximum below the mid-plane if the vertical rate of change of resistivity is positive. This maximum value moves downward with the increasing such magnitude of the

vertical rate of change of resistivity. However, flow amplitude reaches a maximum above the mid-plane if the vertical rate of change of resistivity is negative, and such maximum value moves further upward with the increasing the magnitude of such negative vertical rate of change.

Table 2 Solutions  $\widehat{\theta}_0(z)$  for various  $\gamma_0$

$z$	$\gamma_0 = 0.0$	$\gamma_0 = 0.6$	$\gamma_0 = -0.5$
0.68	0.01362	0.01095	0.01796
0.67	0.01388	0.01118	0.01826
0.66	0.01413	0.01140	0.01855
0.65	0.01437	0.01161	0.01881
0.64	0.01459	0.01181	0.01906
0.63	0.01480	0.01199	0.01928
0.62	0.01499	0.01217	0.01949
0.61	0.01517	0.01233	0.01967
0.60	0.01534	0.01249	0.01983
0.59	0.01549	0.01263	0.01998
0.58	0.01562	0.01276	0.02010
0.57	0.01574	0.01288	0.02020
0.56	0.01584	0.01298	0.02028
0.55	0.01593	0.01307	0.02034
0.54	0.01600	0.01315	0.02038
0.53	0.01605	0.01322	0.02040
0.52	0.01609	0.01328	0.02039
0.51	0.01612	0.01332	0.02038
0.50	0.01613	0.01335	0.02034
0.49	0.01612	0.01336	0.02028
0.48	0.01609	0.01337	0.02020
0.47	0.01605	0.01335	0.02010
0.46	0.01600	0.01334	0.01998
0.45	0.01593	0.01330	0.01984
0.44	0.01584	0.01325	0.01969
0.43	0.01574	0.01319	0.01951
0.42	0.01562	0.01311	0.01932
0.41	0.01549	0.01302	0.01911
0.40	0.01534	0.01292	0.01888
0.39	0.01517	0.01280	0.01864
0.38	0.01499	0.01267	0.01837
0.37	0.01480	0.01253	0.01810
0.36	0.01459	0.01237	0.01780
0.35	0.01437	0.01220	0.01749
0.34	0.01413	0.01202	0.01717
0.33	0.01388	0.01182	0.01683
0.32	0.01362	0.01162	0.01647

Figure 5 displays the two dimensional results for the linear solution  $\Theta_0(x,z)$  for  $\gamma_0 = 0.0$  for one period in  $x$ -direction. For  $\gamma_0 = 0.0$ , The maximum value occurs at the center of the domain, i.e., at  $(0.0, 0.5)$ . The minimums occur in the middle with respect to  $z$ , i.e., at  $z = 0.5$ , and at both ends of the period with respect  $x$ , i.e., at  $x = -1.0$  and  $x = 1.0$ . Result is symmetric with respect to  $x = 0$  and  $z = 0$ . Similar results are observed for the velocity component,  $W_0(x,z)$ .

Computed result for the linear solution of the temperature,  $\Theta_0(x,z)$ , for  $\gamma_0 = 1.4$  and  $\gamma_0 = -1.0$  is shown in Fig.6. The maximum values occur at  $x = 0$  and the minimum values occur at both end of the period with respect to  $x$ . But these values shift towards the bottom of the layer for positive  $\gamma_0$  and

towards the top of the layer for negative  $\gamma_0$ . Similar results are observed for the velocity component,  $W_0(x,z)$ .

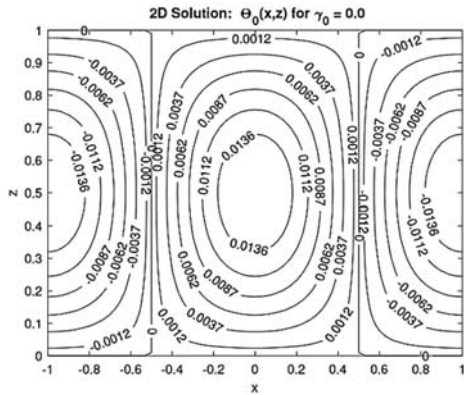


Fig. 5. Linear Solution  $\Theta_0(x,z)$  for  $\gamma_0 = 0.0$ .

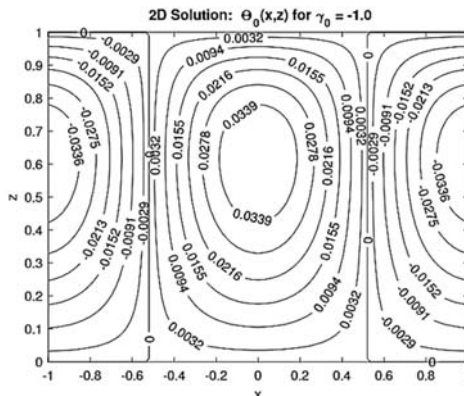
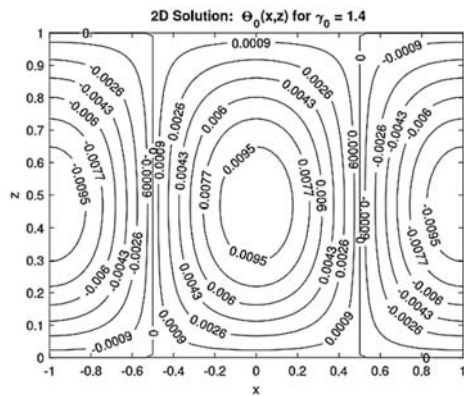


Fig. 6. Linear solution  $\Theta_0(x,z)$  for  $\gamma_0 = 1.4$  and  $\gamma_0 = -1.0$ .

The first-order solutions (one-alpha and two-alpha modes) for the first-order temperatures,  $\Theta_{11}(z)$  and  $\Theta_{12}(z)$ , are displayed in Fig.7. In all computations, we use  $R_1 = 1.0$ . For one-alpha mode, the maximum values of the dependent variables shift down-ward in the layer for positive values of  $\gamma_0$  and the maximum values move upward for negative values of  $\gamma_0$ . But, for two-alpha mode, the maximum values of the dependent variables shift upward for any values of  $\gamma_0$ . Both solutions have smaller values for positive  $\gamma_0$

than those values for  $\gamma_0 = 0$  and have higher values for negative  $\gamma_0$  than the values for  $\gamma_0 = 0$ . Two alpha mode results dominate one alpha mode results for both dependent variables. Similar results hold for the vertical components of the velocity,  $W_{11}(z)$  and  $W_{12}(z)$ .

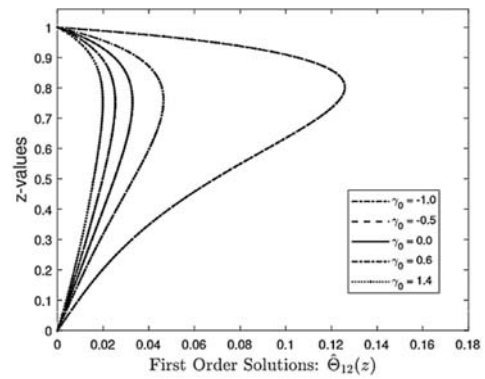
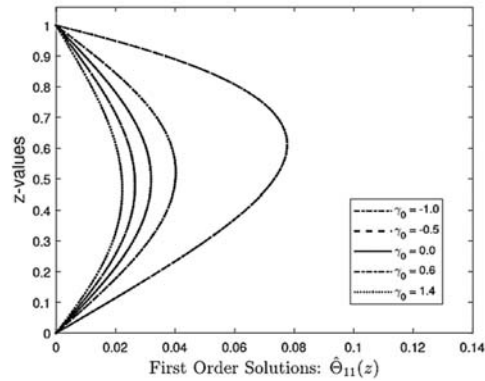


Fig. 7. First-order solutions  $\Theta_{11}(z)$  and  $\Theta_{12}(z)$  for various  $\gamma_0$ .

Figure 8 displays the two dimensional result for the first-order for the temperature,  $\Theta_{11}(x,z)$ , for  $\gamma_0 = 0.0$  for one period in x-direction. The maximum value for is obtained at  $(0.0, 0.5)$ . The minimums occur at  $z = 0.5$ , and at both ends for x, i.e., at  $x = -1.0$  and  $x = 1.0$ . For the one-alpha solution for the velocity component,  $W_{11}(x,z)$ , similar behavior is observed.

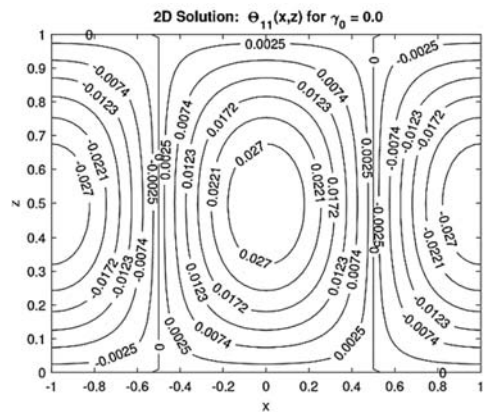


Fig. 8. First-order solution  $\Theta_{11}(x,z)$  for  $\gamma_0 = 0.0$ .



Computed results for the first-order one-alpha solutions for the temperature,  $\Theta_{11}(x,z)$ , for  $\gamma_0 = 1.4$  and  $\gamma_0 = -1.0$  are shown in Fig.9. The maximum values occur at  $x = 0$  and the minimum values occur at both end of the period of  $x$ . But these values shift upward in the layer for negative  $\gamma_0$  and downwards for positive  $\gamma_0$ . Similar results hold for the velocity component,  $W_{11}(x,z)$ .

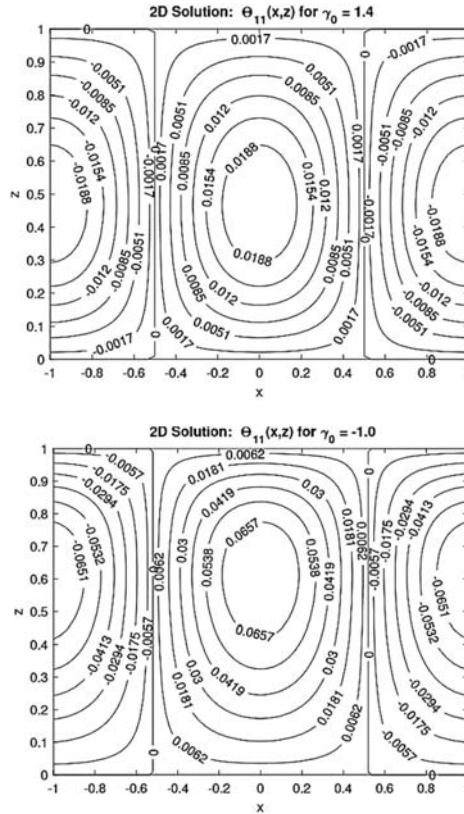


Fig. 9. First-order solutions  $\Theta_{11}(x,z)$  for  $\gamma_0 = 1.4$  and  $\gamma_0 = -1.0$ .

Figure10 shows the solution for the first-order two-alpha mode for the temperature,  $\Theta_{12}(x,z)$ , for  $\gamma_0 = 0.0$ . The maximum and minimum values shift upward. Result is symmetric about  $x = 0$ . Similar result is observed for the velocity component,  $W_{12}(x,z)$ .

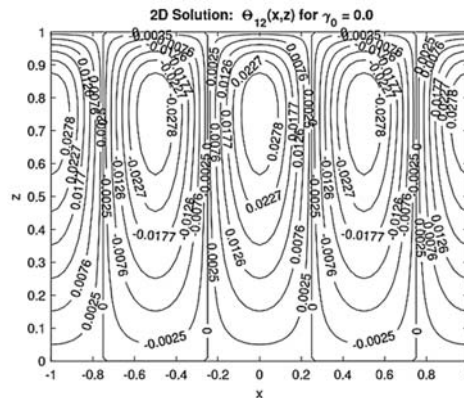


Fig. 10. First-order solution  $\Theta_{12}(x,z)$  for various  $\gamma_0 = 0.0$ .

Table-3 displays the combined first-order temperature  $\widehat{\Theta}_1(z) = \widehat{\Theta}_{11}(z) + \widehat{\Theta}_{12}(z)$  for various  $\gamma_0 = 0.0, 0.6$  and  $-0.5$ .

Table 3 Solution  $\widehat{\Theta}_1(z)$  for various  $\gamma_0$

$z$	$\gamma_0 = 0.0$	$\gamma_0 = 0.6$	$\gamma_0 = -0.5$
0.66	0.05908	0.04667	0.07994
0.65	0.05925	0.04688	0.07997
0.64	0.05938	0.04705	0.07993
0.63	0.05946	0.04720	0.07982
0.62	0.05950	0.04731	0.07965
0.61	0.05949	0.04738	0.07942
0.60	0.05945	0.04743	0.07913
0.59	0.05936	0.04744	0.07878
0.58	0.05923	0.04743	0.07838
0.57	0.05906	0.04738	0.07792
0.56	0.05884	0.04730	0.07741
0.55	0.05860	0.04719	0.07684
0.54	0.05831	0.04706	0.07623
0.53	0.05798	0.04689	0.07557
0.52	0.05761	0.04669	0.07486
0.51	0.05721	0.04646	0.07411
0.50	0.05677	0.04620	0.07331

It is observed from our computational results presented in Table 3 that the first-order solution ( $\widehat{\Theta}_1(z) = \widehat{\Theta}_{11}(z) + \widehat{\Theta}_{12}(z)$ ) has the maximum value of 0.05950 at  $z = 0.62$  for  $\gamma_0 = 0$ . It has a maximum value of 0.07997 at  $z = 0.65$  for  $\gamma_0 = -0.5$ , and a maximum value of 0.04744 at  $z = 0.59$   $\gamma_0 = 0.6$ .

The first-order solutions for the temperature,  $\widehat{\Theta}_1(z)$ , for different values of  $\gamma_0$  are presented in Fig.11. The maximum values shift upward (higher  $z$ ) in the layer for any values of  $\gamma_0$ . Solutions have smaller values for positive  $\gamma_0$  than those values for  $\gamma_0 = 0$  and have higher values for negative  $\gamma_0$  than those for  $\gamma_0 = 0$ . For the vertical component of the velocity,  $\widehat{W}_1(z)$ , similar results are observed.

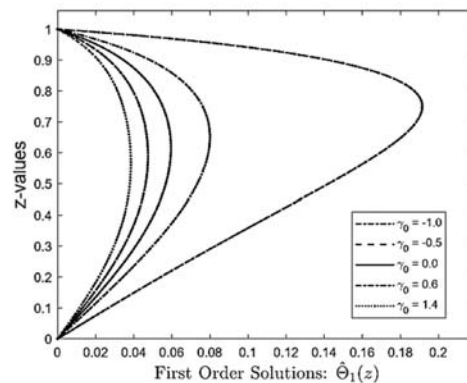


Fig. 11. First-order solution  $\widehat{\Theta}_1(z)$  for various  $\gamma_0$ .

Fig.12 displays the two dimensional results for the first-order (combined one-alpha and two-alpha) solution for the temperature,  $\Theta_1(x,z)$ , for  $\gamma_0 = 0.0$ .

The maximum value occurs at  $x = 0$ . The minimum values for  $\Theta_1(x,z)$  not at the end, but inside the period of  $x$ .

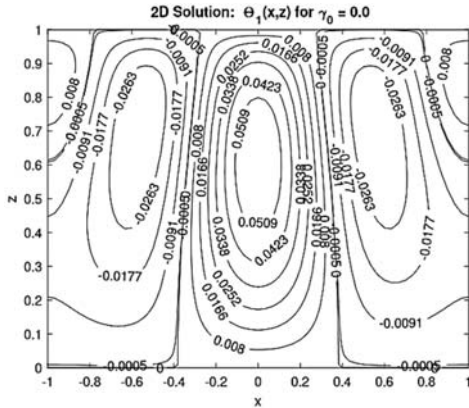


Fig. 12. First-order solution  $\Theta_1(x,z)$  for  $\gamma_0 = 0.0$ .

Results for the first-order solutions for temperature,  $\Theta_1(x,z)$ , for  $\gamma_0 = 1.4$  and  $\gamma_0 = -1.0$  are presented in Fig.13. The maximum and minimum values shift upward in the layer for negative  $\gamma_0$ . Results are symmetric with respect to  $x = 0$ .

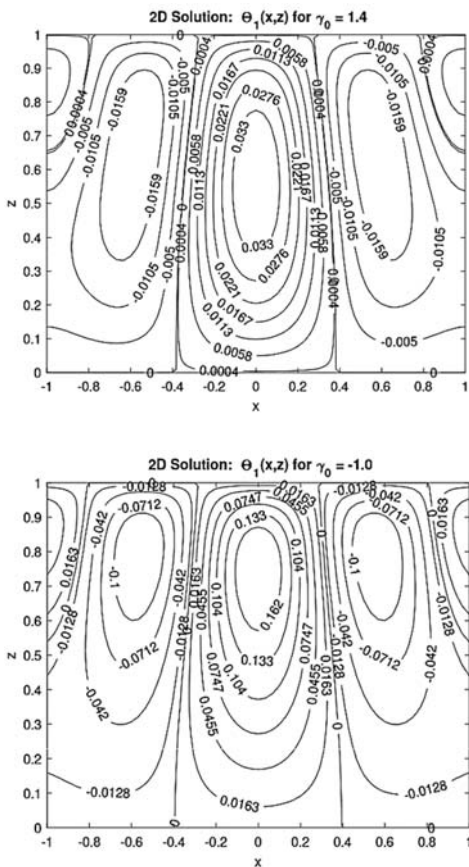


Fig. 13. First-order solutions  $\Theta_1(x,z)$  for  $\gamma_0 = 1.4$  and  $\gamma_0 = -1.0$ .

Table-4 displays the nonlinear temperature  $\widehat{\Theta}_0 + \varepsilon \widehat{\Theta}_1$  for various  $\gamma_0 = 0.0, 0.65$  and  $-0.5$ .

Table 4 Solution  $\widehat{\Theta}_0 + \varepsilon \widehat{\Theta}_1$  for various  $\gamma_0$

$z$	$\gamma_0 = 0.0$	$\gamma_0 = 0.6$	$\gamma_0 = -0.5$
0.66	0.02004	0.01607	0.02654
0.65	0.02029	0.01630	0.02681
0.64	0.02053	0.01651	0.02705
0.63	0.02075	0.01671	0.02727
0.62	0.02094	0.01690	0.02745
0.61	0.02004	0.01707	0.02761
0.60	0.02128	0.01723	0.02775
0.59	0.02142	0.01737	0.02786
0.58	0.02154	0.01750	0.02794
0.57	0.02164	0.01761	0.02799
0.56	0.02172	0.01771	0.02802
0.55	0.02179	0.01779	0.02803
0.54	0.02183	0.01786	0.02800
0.53	0.02185	0.01791	0.02796
0.52	0.02186	0.01794	0.02789
0.51	0.02184	0.01796	0.02779
0.50	0.02180	0.01797	0.02767
0.49	0.02175	0.01795	0.02752
0.48	0.02167	0.01793	0.02736

It is observed from our computational results presented in Table-4 that the nonlinear solution,  $\widehat{\Theta}_0(z) + \varepsilon \widehat{\Theta}_1(z)$ , has the maximum value of 0.02186 at  $z = 0.52$  for  $\gamma_0 = 0$ . We use  $\varepsilon = 0.1$  It has a maximum value of 0.02803 at  $z = 0.55$  for  $\gamma_0 = -0.5$ , and a maximum value of for 0.01797 at  $z = 0.50$   $\gamma_0 = 0.6$ .

Results for the nonlinear temperature,  $\widehat{\Theta}_0(z) + \varepsilon \widehat{\Theta}_1(z)$ , for different values of  $\gamma_0$  are presented in Fig.14. Negative  $\gamma_0$  has destabilizing effect and positive  $\gamma_0$  has stabilizing effect on the flow.

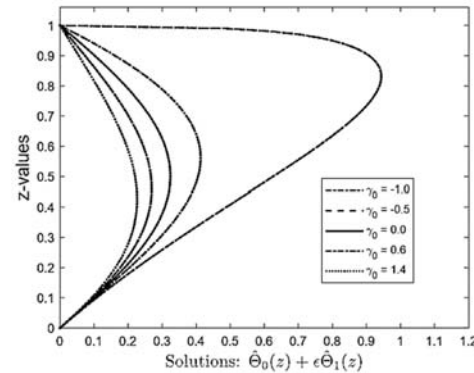


Fig. 14. Linear and first-order combined solutions for temperature.

Figure 15 displays the two dimensional results for  $\Theta_0(x,z) + \varepsilon \Theta_1(x,z)$  for  $\gamma_0 = 0.0$ . The maximum value occurs at  $x = 0$ . The minimum values for  $\Theta_1(x,z)$  appear inside the period of  $x$ , not at the end.

Results for  $\Theta_0(x,z) + \varepsilon \Theta_1(x,z)$  with  $\gamma_0 = 1.4$  and  $\gamma_0 = -1.0$  are presented in Fig.16. The maximum and minimum values shift upward in the layer for



negative  $\gamma_0$ . All the results are symmetric with respect to  $x = 0$ . Similar results are observed for velocity component,  $W_0(x,z) + \epsilon W_1(x,z)$  Here are the highlights of the findings from this work:

- The critical Rayleigh numbers and marginal stability curves indicate that stability region is effected by the resistivity.
- When the vertical rate of change in resistivity,  $\gamma_0$ , is zero, it reduces to the standard problem of constant resistivity where the critical wave number and critical Rayleigh number are known to be  $\pi$  and  $4\pi^2$ , respectively, which match the values computed in Table 1 (3rd column).
- It is observed that for  $\gamma_0 = 0.0$ , the linear solution  $\Theta_0$  has a maximum value at the middle of the layer, and is symmetric about the middle of the layer. The maximum value of  $\Theta_0$  shifts downward in the layer for positive values of  $\gamma_0$  and its maximum value moves upward for negative values of  $\gamma_0$ .
- It is observed that the maximum values for the first-order solution,  $(\Theta_1 = \Theta_{11} + \Theta_{12})$ , shift to the upper half plane for any value of  $\gamma_0$ . At  $x = 0$ , it is observed that the first-order solution has the maximum value of 0.05950 at  $z = 0.62$  for  $\gamma_0 = 0$ . It has a maximum value of 0.07997 at  $z = 0.65$  for  $\gamma_0 = -0.5$ , and a maximum value of for 0.04744 at  $z = 0.59$   $\gamma_0 = 0.6$ .
- The contribution of the linear and first-order solutions to temperature at the middle of the layer ( $z = 0.5$ ) for  $x = 0$ , are 0.02186, 0.01797, and 0.02803 for the respective values 0.0, 0.6, and -0.5 of the resistivity parameter. Computational results for the nonlinear solutions demonstrate that buoyancy force and the resulting convective flow quantities are more effective above the mid-plane  $z = 0.5$  if resistivity is weaker. The convective temperature decreases with increasing resistivity, while it increases with decreasing resistivity.
- For a positive vertical rate of change in resistivity, the flow and temperature are stabilizing and their magnitudes are lower in region near the upper boundary, while for a negative vertical rate of change in resistivity, the flow and temperature are destabilizing and their magnitudes are higher in region near the upper boundary.

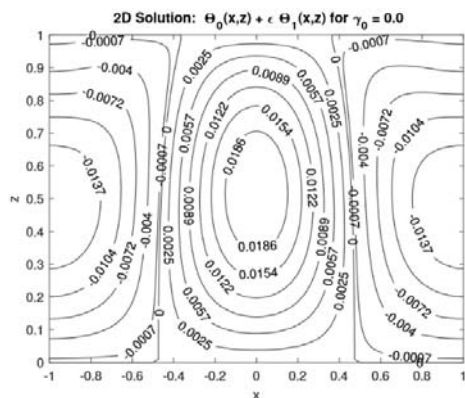


Fig. 15. Linear and first-order combined solution for  $\gamma_0 = 0.0$ .

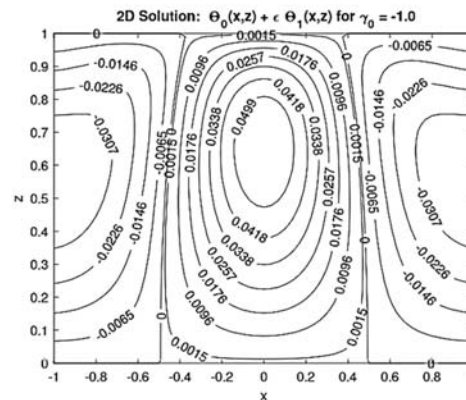
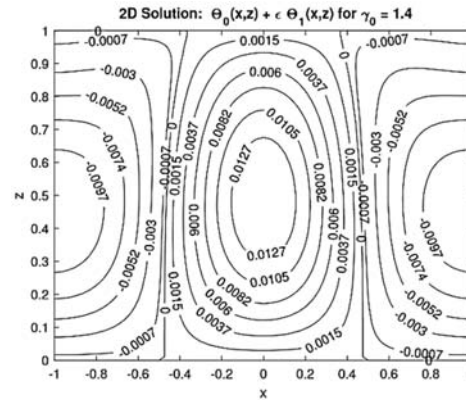


Fig. 16. Solutions  $\Theta_0(x,z) + \epsilon \Theta_1(x,z)$  for  $\gamma_0 = 1.4$  and  $\gamma_0 = -1.0$ .

## 6. SUMMARY AND CONCLUSIONS

Here we study the effect of the vertical rate of change in resistivity on a hydro-thermal convective flow in a porous medium. Based on the critical Rayleigh number and the critical wave number computed from the linear system, we derived the first-order system using weakly non-linear procedure. We used the fourth-order Runge-Kutta method in combination with the shooting method to solve linear and first-order systems numerically. Results indicate a stabilizing effect on the temperature and flow for a positive vertical rate of change in resistivity, whereas a destabilizing effect is noticed for a negative rate of change. It is observed that the convective flow driven by the buoyancy force is more effective if resistivity is weaker, while the opposite result holds for a stronger resistivity effect. Both convective temperature and velocity decrease with increasing resistivity, while they increase with decreasing resistivity.

In addition, flow is asymmetric with respect to the middle of the layer for a non-zero rate of change in resistivity. The maximum values for the temperature and velocity shift downward for a positive vertical rate of change in resistivity and upward for a negative rate of change. Advantage of this study is that it is a first step for future extension to more general variable hydraulic resistivity. The present work also provides understanding the nature of the

nonlinear flow as is affected by presence of variable resistivity whose rate of change is arbitrary. Earlier studies only used small variation. The current study doesn't have that restriction. Disadvantage of the present study is its limitation for linear variation of resistivity, two-dimensionality of the problem, and the more involved nonlinear second order solutions that are not provided. Future studies may include extending the current work to incorporate nonlinear second-order system and three dimensional extension, and stability of such primary flow solutions.

**ACKNOWLEDGMENT**

The authors would like to offer a special thanks to the reviewers for their constructive comments which were very helpful to improve the quality of the paper.

**APPENDIX**

**Elimination of the Pressure**

We eliminate the pressure from the Eq. (10) using the poloidal ( $\mathcal{P}$ ) and toroidal ( $\mathcal{T}$ ) representations of  $\vec{U}$  (since  $\nabla \cdot \vec{U} = 0$ , Chandrasekhar 1981) which is given by

$$\vec{U} = (U, V, W) = -\vec{\mathcal{P}}\phi + \vec{\mathcal{T}}\psi, \text{ where}$$

$$\vec{\mathcal{P}} = \nabla \times \nabla \times \hat{k}, \vec{\mathcal{T}} = \nabla \times \hat{k}$$

Thus, we have  $W = -\Delta_2 \phi$  where  $\Delta_2 = \frac{\partial^2}{\partial x^2} + \frac{\partial^2}{\partial y^2}$ . After elimination of pressure by taking the vertical component of the double curl of the Eq. (10), the perturbed system becomes:

$$\gamma \nabla^2 W + \frac{d\gamma}{dz}(DW) - \mathcal{R}_c(\Delta_2 \theta) = \varepsilon \mathcal{R}_1(\Delta_2 \theta) \quad (25)$$

$$\nabla^2 \theta - W \frac{d\theta_b}{dz} = \varepsilon \vec{U} \cdot \nabla \theta \quad (26)$$

Where  $\nabla^2 = \frac{\partial^2}{\partial x^2} + \frac{\partial^2}{\partial y^2} + \frac{\partial^2}{\partial z^2}$ ,  $D = \frac{\partial}{\partial z}$ . The boundary conditions are  $\theta = W = 0$  at  $z = 0, 1$ .

**2-D Normal Mode Solutions**

Now, we consider the two dimensional case. Using the normal mode approach, we express the linear solutions as

$$[\theta_0(x, z), W_0(x, z)] = \hat{\theta}_0(z), \hat{W}_0(z) e^{i\alpha x}$$

where  $\alpha$  denotes the wave number. Thus, we have

$$\nabla^2 W_0(x, z) = e^{i\alpha x} \left( \frac{d}{dz} - \alpha^2 \right) \hat{W}_0(z)$$

$$\nabla^2 \theta_0(x, z) = e^{i\alpha x} \left( \frac{d}{dz} - \alpha^2 \right) \hat{\theta}_0(z)$$

Using the above equations in the linear system (14)-(15), we obtain

$$(1 + \gamma_0 z) \left( \frac{d^2}{dz^2} - \alpha^2 \right) \hat{W}_0 + \gamma_0 \frac{d\hat{W}_0}{dz} + \alpha^2 \mathcal{R}_c \hat{\theta}_0 = 0$$

$$\left( \frac{d^2}{dz^2} - \alpha^2 \right) \hat{\theta}_0 + \hat{W}_0 \frac{d\theta_b}{dz} = 0 \quad (27)$$

with boundary conditions  $\hat{\theta}_0 = 0 = 0$  at  $z = 0, 1$ .

For the first-order solutions, we have two parts: one is called one-alpha mode due to the presence of  $e^{i\alpha x}$  and the other called two-alpha mode due to the presence of  $e^{2i\alpha x}$ . Thus for the temperature, the first-order solution  $\Theta_1(x, z) = \Theta_{11}(x, z) + \Theta_{12}(x, z)$ , we write

$$[\Theta_{11}, \Theta_{12}] = [\hat{\Theta}_{11}(z) e^{i\alpha x}, \hat{\Theta}_{12}(z) e^{2i\alpha x}]$$

which yield

$$\nabla^2 \theta_{11}(x, z) = e^{i\alpha x} \left( \frac{d^2}{dz^2} - \alpha^2 \right) \hat{\theta}_{11}(z)$$

$$\nabla^2 \theta_{12}(x, z) = e^{i\alpha x} \left( \frac{d^2}{dz^2} - 4\alpha^2 \right) \hat{\theta}_{12}(z)$$

Also for the velocity component, the first-order  $W_1(x, z) = W_{11}(x, z) + W_{12}(x, z)$  where  $W_{11} = \hat{W}_{11}(z) e^{i\alpha x}$  and  $W_{12} = \hat{W}_{12}(z) e^{2i\alpha x}$ , similar results hold.

Now using the above results in the first-order system (16)-(17), we have one-alpha and two-alpha mode systems, respectively, as

$$(1 + \gamma_0 z) \left( \frac{d^2}{dz^2} - \alpha^2 \right) \hat{W}_{11} + \gamma_0 \frac{d\hat{W}_{11}}{dz} + \alpha^2 \mathcal{R}_c \hat{\theta}_{11} = -\alpha^2 \mathcal{R}_1 \hat{\theta}_b$$

$$\left( \frac{d^2}{dz^2} - \alpha^2 \right) \hat{\theta}_{11} + \hat{W}_{11} = 0 \quad (28)$$

with  $\hat{\theta}_{11} = \hat{W}_{11} = 0$  at  $z = 0, 1$  and

$$(1 + \gamma_0 z) \left( \frac{d^2}{dz^2} - 4\alpha^2 \right) \hat{W}_{12} + \gamma_0 \frac{d\hat{W}_{12}}{dz} + 4\alpha^2 \mathcal{R}_c \hat{\theta}_{12} = 0$$

$$\left( \frac{d^2}{dz^2} - \alpha^2 \right) \hat{\theta}_{12} + \hat{W}_{12} = \hat{W}_0 \frac{d\hat{\theta}_{12}}{dz} \quad (29)$$

with  $\hat{\theta}_{12} = \hat{W}_{12} = 0$  at  $z = 0, 1$  and

**REFERENCES**

Aldoss, T. K. (2009). Natural convection from a horizontal annulus filled with porous medium of variable permeability. *Journal of Porous Media* 12, 715-724.

Bhatta, D. and D. N. Riahi (2017). Convective flow in an aquifer layer. *Fluids* 52, 1-19.

Bhatta, D., D. N. Riahi and M. S. Muddamallappa (2010). On nonlinear evolution of convective flow in an active mushy layer. *Journal of Engineering Mathematics* 82, 385-399.

Bhatta, D., M. S. Muddamallappa and D. N. Riahi (2012). Magnetic and permeability effects on a weakly nonlinear magneto-convective flow in an active mushy layer. *International Journal of Fluid Mechanics Research* 39, 494-520.

Chandrasekhar, S. (1981). *Hydrodynamic and Hydromagnetic Stability*, Oxford University Press, Oxford.

Dejam, M. (2018). Dispersion in non-Newtonian fluid flows in a conduit with porous walls. *Chemical Engineering Science* 189, 296-310.

- Dejam, M. (2019a). Derivation of dispersion coefficient in an electro-osmotic flow of a viscoelastic fluid through a porous-walled micro-channel. *Chemical Engineering Science* 204, 298-309.
- Dejam, M. (2019b). Advective-diffusive-reactive solute transport due to non-Newtonian fluid flows in a fracture surrounded by a tight porous medium. *International Journal of Heat and Mass Transfer* 128, 1307-1321.
- Dejam, M. (2019c). Hydrodynamic dispersion due to a variety of flow velocity profiles in a porous-walled microfluidic channel. *International Journal of Heat and Mass Transfer* 136, 87-98.
- Falsaperla, P., G. Mulone and B. Straughan (2010). Modal package convection in a porous layer with boundary imperfections, *International Journal of Engineering Science* 48, 685-692.
- Fowler, A. C. (1997). *Mathematical Models in the Applied Sciences*, Cambridge University Press, Cambridge.
- Fusi, L., A. Farina and F. Rosso (2015). Mathematical models for fluids with pressure-dependent viscosity flowing in porous media. *International Journal of Engineering Science* 87, 110-118.
- Gangadharaiah, Y. H. (2016). Onset of Benard-Marangoni Convection in a Composite Layer with Anisotropic Porous Material. *Journal of Applied Fluid Mechanics* 9(3), 1551-1558.
- Hassanien, I. A. and G. M. Omar (2005). Mixed-convection flow adjacent to a horizontal surface in a porous medium with variable permeability and surface heat flux. *Journal of Porous Media* 8, 225-235.
- Hsiao, S. W. (1998). Natural convection in an inclined porous cavity with variable porosity and thermal dispersion effects. *International Journal of Numerical Methods for Heat & Fluid Flow* 8, 97-117.
- Kincaid, D. and W. Cheney (2002). *Numerical Analysis: Mathematics of Scientific Computing*, Third Edition, American Mathematical Society, Providence, Rhode Island.
- Kou, Z. and M. Dejam (2019). Dispersion due to combined pressure-driven and electro-osmotic flows in a channel surrounded by a permeable porous medium. *Physics of Fluids* 31(5), 056603.
- Muddamallappa, S. M., D. Bhatta and D. N. Riahi (2009). Numerical investigation on marginal stability and convection with and without magnetic field in a mushy layer. *Transport in Porous Media* 79, 301-317.
- Nakshatrala, K. B. and K. R. Rajagopal (2011). A numerical study of fluids with pressure-dependent viscosity flowing through a rigid porous medium. *International Journal of Numerical Methods of Fluids* 67, 342-368.
- Nield, D. A. and A. Bejan (2017). *Convection in a Porous Media*, Fifth Edition, Springer, N.Y.
- Oliveski, R. D. C. and L. D. F Macrczak (2008). Natural convection in a cavity filled with porous medium with variable porosity and Darcy number. *Journal of Porous Media* 11, 255-264.
- Rees, D.A.S. and I. Pop (2000). Vertical free convection in a porous medium with variable permeability effects. *International Journal of Heat & Mass Transfer* 43, 2565-2571.
- Riahi, D. N. (1989). Nonlinear convection in a porous layer with permeable boundaries, *International Journal Nonlinear Mechanics* 24, 459-463.
- Riahi, D. N. (1996). Modal package convection in a porous layer with boundary imperfections, *Journal of Fluid Mechanics* 318, 107-128.
- Riahi, D. N. (2009). On oscillatory modes of nonlinear compositional convection in mushy layers. *Nonlinear Analysis: Real World Applications* 10, 209-226.
- Rubin, H. (1981). Onset of thermohaline convection in heterogeneous porous media. *Israel Journal Tech.* 19, 110-117.
- Rubin, H. (1982). Thermohaline convection in a nonhomogeneous aquifer. *Journal of Hydrology* 57, 307-320.
- Tait, S., K. Jahrling and C. Jaupart (1992). The planform of compositional convection and chimney formation in a mushy layer. *Nature* 359, 406-408.
- Vafai, K. (1984). Convective flow and heat transfer in variable-porosity media. *Journal of Fluid Mechanics* 147, 233-259.
- Vafai, K. (2005). *Handbook of Porous Media*, Second Edition, Edited, Taylor & Francis, Boca Raton, FL.
- Wang, Y., X. Xia, Y. Wang, L. Wang and W. Hu (2017). Using proper orthogonal decomposition to solve heat transfer process in a flat tube bank fin heat exchanger. *Adv. Geo-energ. Res.* 1 (3), 158-170.